The Journal of Green Energy and Environmental Engineering

Research Paper

Removal of Heavy Metal Ions by Activated Carbon Modified by Calcium

Emily Leese[1], Christopher Genesan[1], Fatma Singhal[2], Peer Azadi[1,*]

[1] Department of Chemical Engineering and Applied Chemistry, Pulp & Paper Centre, University of Toronto, 200 College Street, Toronto, Ontario M5S 3E5, Canada
[2] Department of Engineering and Mathematical Sciences, School of Agricultural and Veterinary Sciences, São Paulo State University (Unesp), Jaboticabal, São Paulo, Brazil
*Corresponding author: e.leese@utoronto.ca

Abstract. The migration and transformation of heavy metal ions in environment, especially water bodies, have been a focal research topic in environmental science. Particularly in alkaline environments, the mobility and bioavailability of Arsenic (As) are relatively high, increasing the complexity of remediation. Activated carbon, owing to its rich pore structure and good stability, is widely used in the remediation of heavy metal-contaminated water bodies. However, its ability to immobilize As is limited by electrostatic repulsion caused by its surface negative charge. Studies have shown that introducing cations can effectively enhance the immobilization capacity of activated carbon for As. Calcium (Ca) has become a key research focus due to its high affinity for As. Nevertheless, the interaction mechanisms between different components of activated carbon and As in the presence of calcium under alkaline conditions remain unclear, and the immobilization effects of activated carbon loaded with different forms of calcium-based materials require further investigation. The main experimental results showed that activated carbons, labeled BC and CBC, were prepared by pyrolysis of wheat straw without and with calcium carbonate addition, respectively, at 850°C. Adsorption results indicated that the adsorption of As(V) by both BC and CBC conformed to the Langmuir isotherm model, characteristic of monolayer adsorption, with theoretical maximum adsorption capacities of 536.3 $mg \cdot g^{-1}$ and 610.0 $mg \cdot g^{-1}$, respectively. The adsorption kinetics for both followed the pseudo-second-order model and were controlled by intraparticle diffusion. Thermodynamic analysis revealed that the adsorption processes of As(V) onto BC and CBC were spontaneous, endothermic, and accompanied by an increase in entropy. Mechanistic studies indicated that the removal of As(V) by BC and CBC primarily relied on co-precipitation.

Keywords: *Activated Carbon, Straw, Calcium Carbonate, Arsenic, Removal*

Received on 05 June 2024, Accepted on 11 August 2024, Published on 15 September 2024

1 Introduction

Arsenic (As) exhibits high toxicity and strong carcinogenicity to organisms. The World Health Organization (WHO) has listed As among the top ten chemicals of major public health concern [1]. Research indicates that arsenite (As(III)) can permeate into tissue cells of the liver, testis, and kidney through transporters of glucose and aquaglyceroporins (such as GLUT1 and GLUT4), while arsenate (As(V)), due to the high structural and charge similarity between the arsenate anion (AsO_4^{3-}) and phosphate (PO_4^{3-}), primarily enters cells via phosphate transporters [2]. Long-term exposure to arsenic environments exceeding 10 μg/L increases susceptibility to liver cancer, skin cancer, cardiovascular diseases, etc. [3]. For example, long-term consumption of water contaminated with 50 μg/L arsenic increases lung cancer risk by 54%, with a further 0.032% increase in risk per 1 μg/L rise in arsenic concentration [4]. Reducing arsenic in drinking water to below 1 μg/L could save 7.63−14.84 million annually in health-related costs [5]. Thus, controlling arsenic pollution is crucial for public health, and effective remediation measures are urgently needed.

Activated carbon is a carbon-rich solid material that can be produced through natural processes or artificial methods. Naturally formed activated carbon is mainly associated with forest and grassland fires, generated as carbonaceous residues under oxygen-limited or low-oxygen conditions. These residues persist in soil long-term, aiding in restoring soil structure, improving water retention, promoting microbial community succession, and playing a significant role in the global carbon cycle [6-8]. In contrast, artificially produced activated carbon has a

wide range of sources, primarily utilizing agricultural and forestry waste, plant residues, and animal manure as raw materials. It is produced under controlled conditions using techniques like pyrolysis, gasification, and hydrothermal carbonization, giving it advantages in pore structure, specific surface area, and chemical composition, making it suitable for environmental remediation and agricultural improvement [9-10].

Activated carbon influences arsenic speciation transformation through multiple mechanisms, including adsorption, precipitation, redox reactions, microbial regulation, and the action of dissolved organic matter. For instance, under specific conditions, activated carbon can promote the formation of insoluble complexes between arsenic and calcium or iron, thereby achieving precipitation. Additionally, activated carbon can act as an electron shuttle in redox processes. For example, when activated carbon loaded with iron and manganese forms oxygen-containing functional groups like Mn-O and Fe-O on its surface, Mn can oxidize As(III) to the more stable As(V) [11]. Microbial activity is also a key mechanism by which activated carbon affects arsenic transformation. It can alter soil microbial community structure and regulate the expression of key genes, promoting the arsenic reduction activity of bacteria such as Geobacter. In some cases, the synergy between lactate and activated carbon can even stimulate the reduction of As(V) to As(III), increasing arsenic bioavailability in soil [12]. The dissolved organic matter (DOM) released by activated carbon is rich in humic-like substances and reactive oxygen-containing functional groups. These components create complex interactions between solid and liquid phases, altering arsenic speciation distribution through redox and complexation reactions, and promoting the transformation of mineral-bound arsenic species [13]. The molecular composition of DOM, particularly humic and lignin-like compounds, plays a decisive role in the redistribution of As(V) and can slowly release arsenic from arsenic-bearing minerals under acidic conditions, further influencing its environmental behavior [14].

Calcium ions (Ca^{2+}), common cations in the environment, can significantly influence arsenic speciation transformation and toxicity mitigation through various mechanisms. On one hand, calcium can promote the binding of arsenic to mineral surfaces like iron oxides and aluminum oxides, leading to the formation of poorly soluble precipitates, thereby reducing its solubility and mobility in water. Simultaneously, calcium can mineralize with arsenic to form stable calcium arsenate minerals (e.g., calcium arsenate, apatite), further reducing its ecological risk. For example, it was [15] found that at pH 6.5, activated carbon-enhanced calcium precipitation increased the removal rate of As(III) to 58.1%, forming $Ca_5(AsO_4)_3OH$ precipitate, significantly reducing arsenic solubility. On the other hand, calcium-modified materials (e.g., calcium-modified activated carbon) also possess strong arsenic adsorption capacity and can promote the conversion of trivalent arsenic to pentavalent arsenic [16], thereby reducing arsenic toxicity and mobility. Therefore, this study uses wheat straw with calcium carbonate as raw materials to prepare calcium-rich modified activated carbon via co-pyrolysis, aiming to efficiently remove As(V) from water bodies and expand the application potential of Ca-modified activated carbon in treating arsenic contamination in alkaline environments.

2 Materials and Methods

2.1 Preparation of Activated Carbon

Calcium carbonate-modified activated carbon was prepared using calcium carbonate reagent as the modifying material. The pretreatment was as follows: sieved wheat straw powder (through a 100-mesh sieve) was uniformly mixed with calcium carbonate powder at a weight ratio of 1:1. The material was mixed in a tube furnace and pyrolyzed under a N_2 atmosphere at a heating rate of 20°C·min^{-1} to 850°C, holding for 2 hours. After pyrolysis, the product was allowed to cool naturally to room temperature, then finely ground using an agate mortar and uniformly sieved through a 200-mesh sieve. The final activated carbon products were named BC (activated carbon) and CBC (calcium carbonate-modified activated carbon) based on the raw materials, and stored sealed in clean centrifuge tubes to ensure material purity.

2.2 Isothermal Adsorption Experiments

Isothermal Adsorption Experiments: As(V) solutions with different concentrations (range 0-1000 mg/L) were prepared. The initial pH of the As(V) solutions was adjusted to 11.0 ± 0.1 using 1 mol·L^{-1} HCl or NaOH. 0.1 g of adsorbent was uniformly mixed with the different concentrations of As(V) solution and stirred at room

temperature for 24 hours using a multi-point magnetic stirrer. The mixture after adsorption equilibrium was filtered, and the supernatant was collected and stored in centrifuge tubes. The As(V) concentration in the supernatant was detected to estimate adsorption capacity of biochar for As(V).

2.3 Kinetic Adsorption Experiments

An As(V) solution (700 mg/L) was prepared. And initial pH of adsorption was adjusted to 11.0 ± 0.1. Besides, 0.1 g of adsorbent was fully mixed with the solution in a 100 mL beaker and placed on a multi-point magnetic stirrer for the adsorption experiment. Samples were taken at different incubation times (10, 60, 120, 240, 480, 720, 1440 minutes), and the residual As(V) in the filtrate was detected to evaluate the adsorption capacity (q_t) of the modified biochar for As(V) at time t. Kinetic models were fitted to the data.

2.4 Effect of pH on As(V) Removal

At room temperature, 100 mg adsorbent was added to 100 mililiter of As(V) solution in a 100 mL beaker. Besides, initial pH of As solution was adjusted to 7.0 ± 0.1, 8.0 ± 0.1, 9.0 ± 0.1, 10.0 ± 0.1, 11.0 ± 0.1, and 12.0 ± 0.1, respectively. Effect of pH value on the adsorption efficiency of As(V) by the adsorbent was investigated, and the adsorption capacity was calculated.

2.5 Effect of co-existing irons on As(V) Removal

A certain concentration of As(V) solution (reference from kinetic experiments) was prepared. Interfering ions (SO_4^{2-}, HCO_3^-, NO_3^-, Cl^-, $H_2PO_4^-$) at concentrations of 0.01 mol·L^{-1} and 0.1 mol·L^{-1} were added separately to simulate real wastewater. The adsorbent dosage was set at 0.1 g, and the solution pH was adjusted to 11.0 ± 0.1. The activated carbon and 100 mL of the mixed solution were added to a 100 mL beaker. The influence of these interfering ions on the adsorption efficiency of arsenate by the adsorbent in aqueous solution was investigated, and the adsorption capacity for As(V) was calculated.

2.6 Determination of Heavy Metal Ions

Determination of Total Arsenic Concentration in Samples: 5 mL of filtered reaction solution was placed in a 25 mL colorimetric tube. 0.1 mL of 11% hydrochloric acid solution and 0.1 mL of 2 mmol·L^{-1} potassium iodate solution were added. After shaking and standing for 1 hour, As(III) in the solution was oxidized to As(V). Then, 0.8 mL of prepared molybdenum-antimony reagent and 1 mililiter of freshly prepared As acid solution were added, and the volume was made up to 10 mL with deionized water. After standing at room temperature for 1 hour, the absorbance of the solution was measured at a wavelength of 870 nm using a spectrophotometer, with a blank experiment conducted simultaneously. After measuring the absorbance, a standard curve was constructed, and the corresponding sample concentration was determined from the absorbance value on the standard curve.

Determination of As(V) Concentration in Samples: The procedure was the same as for total As determination, except that the 11% hydrochloric acid and potassium iodate solutions were not added. As(III) concentration was expressed as the gap between total As and As(V).

The concentration of Ca^{2+} in this experiment was determined using flame atomic absorption spectrometry.

2.7 X-ray Diffraction (XRD)

XRD was characterized using a Bruker D8 Advance X-ray diffractometer (Germany) for phase analysis and crystallinity determination. The experiment used a Cu Kα radiation source (λ = 0.15418 nm), with operating voltage and current set at 40 mA and 40 kV, respectively. The scanning mode was continuous step scanning with a speed of 10 °·min^{-1}, step size of 0.05 °, and the diffraction angle (2θ) scanning range set from 3° to 85°.

2.8 Fourier Transform Infrared Spectroscopy (FTIR)

Surface functional groups of the materials were characterized using a PerkinElmer Spectrum Two FTIR spectrometer (USA). Samples were prepared using the potassium bromide pellet method, and full-spectrum scanning was performed in the wavenumber range of 4000-400 cm^{-1}.

2.9 SEM-EDS determination

Surface morphology of biochar were characterized by scanning electron microscopy (SEM-EDS, Hitachi su8100 cold field SEM) equipped with energy dispersive X-ray spectroscopy (EDS), HITACHI， Japan).

2.10 XPS determination

The thermal scientific escalab 250 Xi spectrometer was used for X-ray photoelectron spectroscopy measurement. The binding energy of C 1s peak of exotic carbon was 284.8 EV when excited by Al K α X-ray.

3 Results and Discussion

3.1 Isothermal Adsorption of As(V) by Calcium Carbonate-Modified Activated Carbon

The adsorption behavior of BC and CBC under different initial As(V) concentrations is shown in Figure 1. For both materials, the adsorption capacity enhanced remarkably with increasing initial As(V) concentration and gradually reached equilibrium. For BC, when the initial concentration reached 600.0 mg/L, the adsorption capacity stabilized at 536.3 mg/g, indicating that the material had reached saturation adsorption at this concentration. In contrast, the adsorption equilibrium for CBC occurred at a higher initial concentration of 700.0 mg/L, with a corresponding maximum adsorption of 610.0 mg/g, demonstrating a stronger As(V) removal capability compared to BC, possibly due to its higher calcium oxide content [17].

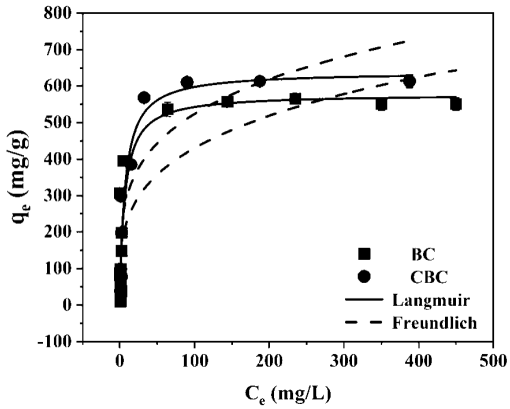

Figure 1 Isotherm fitting curve of As(V) on BC and CBC

3.2 Kinetics of As(V) Adsorption by Calcium Carbonate-Modified Activated Carbon

As shown in Figure 2, BC and CBC exhibited different kinetic characteristics for As(V) adsorption over different time scales. In adsorption with an initial As(V) concentration of 600 mg/L, the adsorption capacity of BC increased rapidly, showing an approximately linear growth within 0-10 minutes, and the adsorption process tended to equilibrium at 120 minutes, indicating a relatively fast adsorption rate for As(V). In the experiment with an starting As(V) concentration of 700 mg/L, the adsorption rate of CBC was relatively slower. Although the adsorption capacity increased rapidly within 0-120 minutes, the equilibrium time was longer, with the adsorption process stabilizing only after 480 minutes, suggesting some hysteresis in its adsorption kinetics.

Results of the kinetic models showed that the regression coefficient (R^2) of the pseudo second order kinetic model was greater than that of the first order model, indicating that the pseudo second order model more accurately describes the As(V) adsorption process. According to adsorption theory for porous materials, the second-order kinetic model assumes that the adsorption rate is determined by the square of the number of unoccupied adsorption sites on the adsorbent surface, suggesting that the process is dominated by chemical adsorption mechanisms, such as coordination bonding, ion exchange, or precipitation reactions. Since BC and CBC possess a large number of calcium-based active sites, their adsorption process exhibits rapid reaction characteristics, reaching equilibrium quickly. This is likely due to strong chemical interactions [18], particularly

the formation of Ca-As precipitates, during As(V) adsorption by BC and CBC. However, it is noteworthy that the first-order kinetic model still showed a relatively high fit, indicating that physical diffusion also plays a role in the adsorption process. Specifically, physical-diffusion is primarily driven by van der Waals forces, a relatively weak interaction suitable for explaining the initial adsorption of As(V) by the microporous structure of the activated carbon surface. Therefore, overall, the adsorption of As(V) by calcium-modified activated carbon is a process driven by both physical diffusion and chemical-adsorption, with chemical-adsorption being dominant, while physical diffusion still significantly influences the adsorption rate [19].

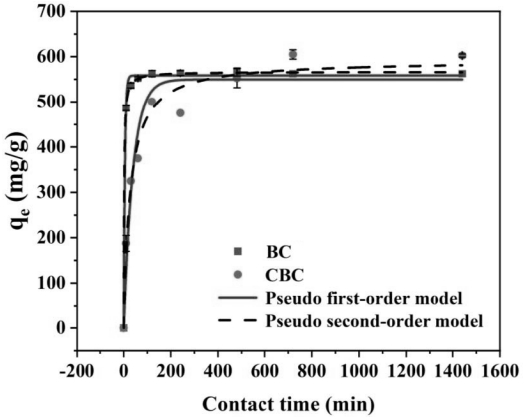

Figure 2 Kinetic fitting curve of As(V) on BC and CBC

3.3 Effect of pH on As(V) Adsorption by Calcium Carbonate-Modified Activated Carbon

Effect of starting pH on As(V) adsorption by the activated carbons is illustrated in Figure 3. Overall, the adsorption of both BC and CBC peaked at pH=9 (571.3 mg/g and 635.0 mg/g, respectively). BC reached its lowest value at pH=12 (552.5 mg/g), while CBC reached its lowest at pH=7 (603.8 mg/g). When the pH-value enhanced from 7 to 9, the adsorption of both materials for As(V) increased. After pH 9, although CBC's adsorption capacity showed a slight rebound at pH=11, the overall trend for both was decreasing. The dynamic change between adsorption capacity and pH is likely influenced by As(V) speciation, activated carbon surface properties, and ion competition in the solution. When pH is between 7 and 11.5, As(V) primarily exists as $HAsO_4^{2-}$; when pH increases to 12, the proportion of AsO_4^{3-} increases significantly. $HAsO_4^{2-}$ might bind more easily with active sites (e.g., Ca^{2+}) on the activated carbon surface compared to AsO_4^{3-}. Furthermore, the activated carbon is loaded with CaO, which forms $Ca(OH)_2$ in water, dissociating into Ca^{2+} and OH^-. Ca^{2+} can react with arsenic anions to adsorb As(V) via precipitation [20]. At pH=9, the Ca^{2+} concentration is moderate, and the OH^- concentration is not yet high enough to compete excessively, resulting in optimal adsorption. When pH increases (e.g., pH=10-12), the OH^- concentration rises, potentially combining with Ca^{2+} to form $Ca(OH)_2$ precipitate, reducing the available Ca^{2+} for As(V) adsorption, thus decreasing the adsorption capacity. Additionally, the activated carbon surface may become negatively charged at high pH, which is unfavorable for adsorbing negatively charged arsenate anions, possibly contributing to the decreased adsorption at higher pH.

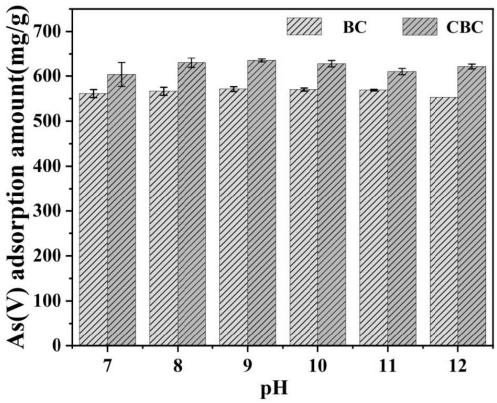

Figure 3 Effect of pH-value on adsorption performance of BC and CBC

3.4 Effect of Co-existing Ions on As(V) Adsorption by Calcium Carbonate-Modified Activated Carbon

The influence of co-existing ions on As(V) adsorption by the activated carbons is shown in Figure 4. Overall, the trend of the effect of co-existing ions was consistent for BC and CBC. For BC, the adsorption was 536.3 mg/g without coexisting ions, while for CBC, it was 610.0 mg/g. In the presence of Cl^- and NO_3^-, the adsorption capacity slightly decreased but remained near the original level, with little difference between the two concentrations (0.01 mol/L and 0.1 mol/L). This might be due to weak interference from Cl^- in competing for adsorption sites with As(V). The presence of SO_4^{2-} had a greater impact on adsorption capacity [21], especially at the 0.1 mol/L concentration, where the adsorption capacity increased significantly. This might indicate that SO_4^{2-} promotes As(V) adsorption through some synergistic effect, such as pH adjustment or changes in surface charge. $H_2PO_4^-$ had the most significant effect, causing a substantial decrease in adsorption capacity to approximately 500-550 mg/g, with a more pronounced decrease at 0.1 mol/L. This suggests strong competition for adsorption sites between $H_2PO_4^-$ and As(V), as both are anions with similar chemical properties, likely sharing common adsorption mechanisms. The presence of HCO_3^- caused the adsorption capacity to drop almost to zero, indicating a very strong inhibitory effect of HCO_3^- on As(V) adsorption. This is probably because HCO_3^- significantly alters the solution pH under alkaline conditions or greatly reduces As(V) adsorption efficiency by competing for adsorption sites [22]. Regarding the concentration effect, for most ions (Cl^-, NO_3^-, SO_4^{2-}), the two concentrations (0.01 mol/L and 0.1 mol/L) had a small and insignificant effect on adsorption capacity. However, for $H_2PO_4^-$ and HCO_3^-, the inhibitory effect was stronger at 0.1 mol/L than at 0.01 mol/L, indicating more intense competition for adsorption sites at higher concentrations of these ions.

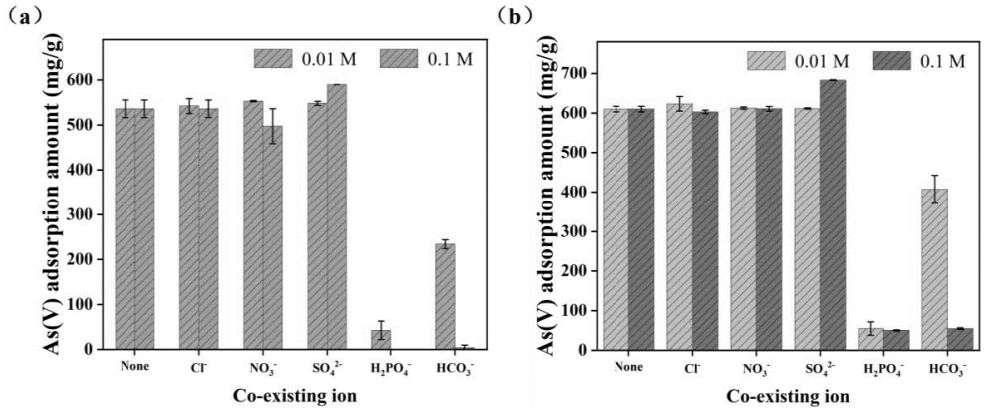

Figure 4 Effect of coexisting ions on As(V) adsorption by BC (a) and CBC (b)

3.5 Mechanism of As(V) Adsorption by Calcium Carbonate-Modified Activated Carbon

Figure 5 shows the SEM-EDS images of BC and CBC. After modification, the surface roughness of biochar increased, more flake crystals appeared, and the specific-surface-area (SSA) of biochar was increased The surface elements of CBC were analyzed by EDS, and it was found that CBC was rich in C and O elements, and its atomic percentage and element mass ratio were 42.76% and 38.01%, respectively, and there were mg, Ca and P elements The mass ratio of Ca element is 11.37%, which indicates that the iron modification of biochar is successful BC and cwbc retain most of the biomass structure, and the surface is composed of many regular and vertical strip-shaped porous structures. The pore structure is very rich and orderly, which is conducive to the adsorption of pollutants BC and CBC are mostly irregular blocks, and the pore structure is honeycomb, which provides rich sites for the adsorption of As.

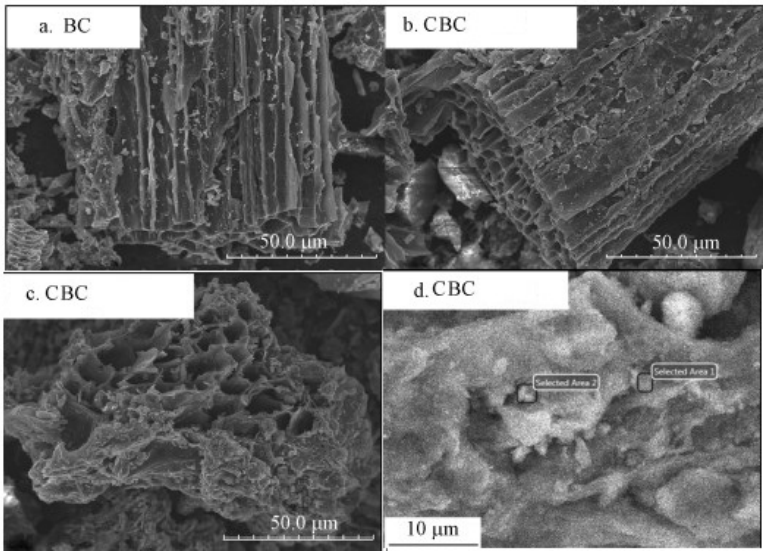

Figure 5 SEM-EDS images of BC and CBC

To investigate the specific changes during the adsorption of As(V) by calcium carbonate-modified activated carbon, XRD characterization was performed on BC and CBC samples before and after adsorption (Figure 6a). The figure shows that before As(V) adsorption, both BC and CBC contained highly crystalline calcium oxide, along with a small characteristic peak of $Ca(OH)_2$. After As(V) adsorption, the intensity of the calcium oxide diffraction peaks disappeared, and relatively distinct characteristic peaks related to Ca-As precipitation appeared due to chemical reactions [23].

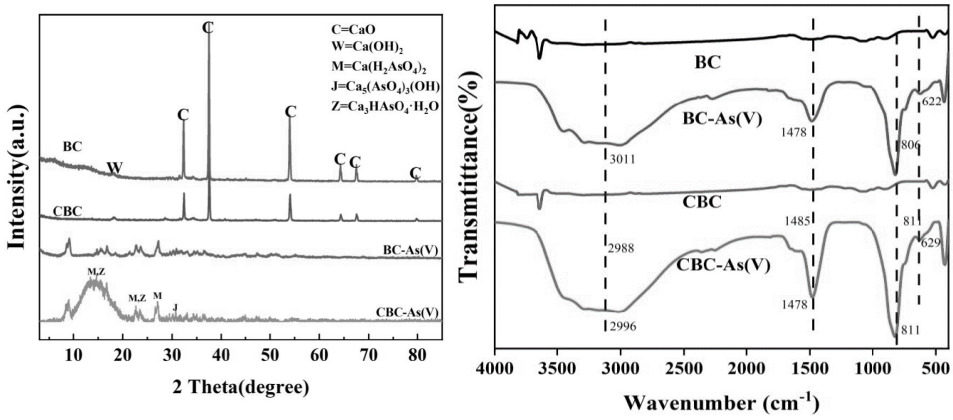

Figure 6 XRD patterns (a) and FTIR spectra (b) of BC and CBC before and after As(V) adsorption

FTIR spectra of the materials are shown in Figure 6b. By comparing the spectral changes before and after adsorption, new characteristic peaks appeared in the range of 2990-3100 cm^{-1} after As(V) adsorption, attributable to -OH functional groups. This might be related to hydroxyl groups in the Ca-As precipitates containing hydroxide formed after the reaction between Ca^{2+} and As(V), or to associated water molecules. Additionally, a new vibration peak appeared at 1478 cm^{-1}, attributed to CO_3^{2-}, indicating the involvement of carbonate ions during the adsorption process. Furthermore, an As-O stretching-vibration peak was found at 811 cm^{-1}, and a Ca-O stretching-vibration peak was found at 629 cm^{-1}, further confirming the adsorption behavior of As(V) on the material surface [24].

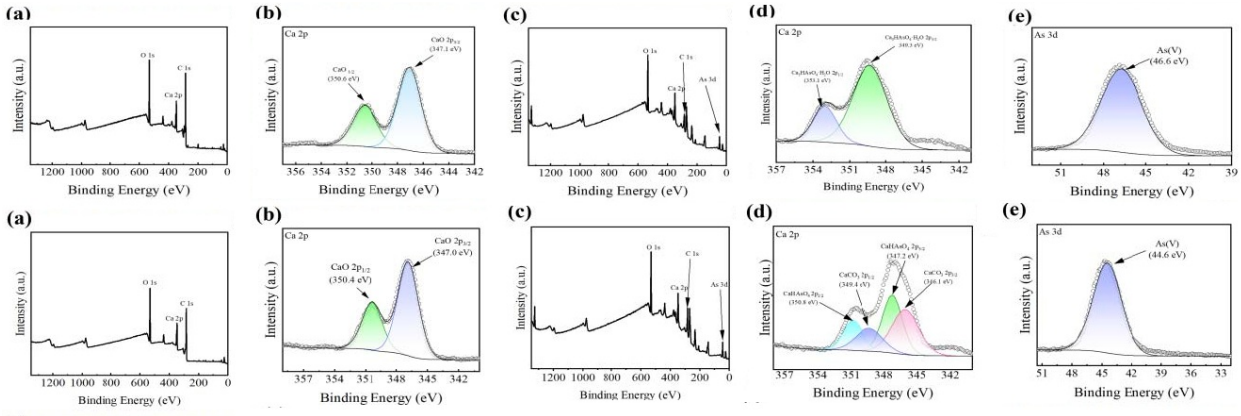

Figure 7 XPS spectra of BC (top) and CBC (bottom) before and after As(V) adsorption: (a)(c) Full spectrum, (b)(d) Ca 2p, (e) As 3d

XPS analysis of BC and CBC materials after As(V) adsorption is shown in Figure 7. After As(V) adsorption, an As 3d peak appeared in the full survey scans of the materials, showing that arsenic was adsorbed onto the modified activated carbons [25]. The Ca 2p atomic orbital can be split into Ca $2p_1/_2$ and Ca $2p_3/_2$, with corresponding peak positions at 353.1 eV and 349.3 eV (Figure 6), indicating the presence of Ca-As precipitates in the materials. Moreover, the As 3d spectrum showed that arsenic existed in the pentavalent state, indicating that no redox reaction occurred during adsorption. It is noteworthy that some characteristic peaks of $CaCO_3$ appeared in CBC , which might be due to the higher concentration of Ca added in CBC [26].

4 conclusion

This chapter primarily investigated the adsorption effectiveness of calcium oxide-loaded activated carbons (BC and CBC) modified with calcium carbonate on As(V), identified the optimal adsorption conditions, and conducted fitting analyses using adsorption kinetics and isotherm models for the As(V) adsorption process by BC and CBC. Furthermore, analyses were performed on the morphological characteristics, crystal structure, surface functional groups, and changes in surface elemental valence states of the modified activated carbons before and after adsorption to explore the underlying mechanisms. The main conclusions are as follows:

Isothermal adsorption fitting results indicated that the adsorption process of As(V) onto CBC conforms to the Langmuir isotherm model, suggesting homogeneous monolayer adsorption. Kinetic adsorption fitting results showed that CBC reached adsorption equilibrium for As(V) at 480 min, following the pseudo-second-order kinetic model, controlled by chemical reactions, with intraparticle diffusion being the main rate-limiting factor. Thermodynamic experiments revealed that the adsorption of As(V) by CBC is spontaneous, endothermic, and accompanied by an increase in entropy. In the initial pH effect experiment, the adsorption capacity first increased and then decreased with increasing pH. In the coexisting ions experiment, $H_2PO_4^-$ and HCO_3^- strongly inhibited the adsorption of As(V). Characterization by XRD, FTIR, and XPS before and after As(V) adsorption on BC and CBC indicated that the primary mechanism for As(V) adsorption by both BC and CBC is co-precipitation.

References

[1] Zheng, K., Chen, Q., Wang, Y., Kang, C. & Xie, L. (2021). Unsupervised Congestion Status Identification Usi ng LMP Data. IEEE Transactions on Smart Grid, 12(1), 726-736. DOI: 10.1109/TSG.2020.3011266.

[2] Liu, Z., Wen, F., & Ledwich, G. (2019). Optimal planning of distributed generation in distribution networks: Models, methods, and future research. Renewable and Sustainable Energy Reviews, 93, 535-545. DOI:10. 1016/j.rser.2018.05.031

[3] Liu, Y., Wang, K., Wang, S., & Wang, Y. (2018). A novel multi-objective optimization model for microgrid sc heduling considering demand response and distributed generation uncertainty. Applied Energy, 230, 421-431. DOI:10.1016/j.apenergy.2018.09.008

[4] Zhang, H., Li, S., & Wang, L. (2019). A deep reinforcement learning based approach for peer-to-peer energ y trading in a microgrid. Applied Energy, 259, 114214. DOI:10.1016/j.apenergy.2019.114214
[5] Zhang, D., Shah, N., & Papageorgiou, L. G. (2018). Efficient energy consumption and operation manageme nt in a smart building with microgrid. Applied Energy, 220, 1-25. DOI:10.1016/j.apenergy.2018.03.101
[6] Zeng, B., & Zhao, L. (2018). Solving two-stage robust optimization problems using a column-and-constrain t generation method. Operations Research Letters, 46(2), 267-273. DOI:10.1016/j.orl.2018.01.007
[7] Fang, X., Misra, S., Xue, G., & Yang, D. (2018). Smart grid—The new and improved power grid: A survey. IE EE Communications Surveys & Tutorials, 14(4), 944-980. DOI:10.1109/SURV.2011.101911.00087
[8] Tan X, Liu Y, Zeng G, et al. Application of biochar for the removal of pollutants from aqueous solutions[J].C hemosphere,2015,125:70-85.
[9] Morstyn, T., Farrell, N., Darby, S. J., & McCulloch, M. D. (2018). Using peer-to-peer energy-trading platfor ms to incentivize prosumers to form federated power plants. Nature Energy, 3(2), 94-101. DOI:10.1038/s 41560-017-0075-y
[10] Dong, Y., Li, Q., & Zhang, Z. (2020). Stochastic optimal scheduling of microgrid with renewable generation and demand response using chance-constrained programming. Applied Energy, 262, 114455. DOI:10.101 6/j.apenergy.2020.114455
[11] Fu, Y., Guo, X., Mi, Y., Yuan, M., Ge, X., Su, X., & Li, Z. (2021). The distributed economic dispatch of smart g rid based on deep reinforcement learning. IET Generation, Transmission & Distribution, 15(18), 2645-265 8. DOI:10.1049/gtd2.12206
[12] Qiu Y, Zhang Y, Zhang K, et al. Intermediate soil acidification induces highest nitrous oxide emissions[J].Na ture Communications, 2024, 15 (1):2695.
[13] Albarakati, A. J., Boujoudar, Y., Azeroual, M., Jabeur, R., Aljarbouh, A., El Moussaoui, H., Lamhamdi, T., & Ouaaline, N. (2021). Real-Time Energy Management for DC Microgrids Using Artificial Intelligence. Energi es, 14(17), 5307. DOI:10.3390/en14175307
[14] Lim, W. Y. B., Luong, N. C., Hoang, D. T., Jiao, Y., Liang, Y., Yang, Q., Niyato, D., & Miao, C. (2020e). Federat ed Learning in Mobile Edge Networks: A Comprehensive survey. IEEE Communications Surveys & Tutorial s, 22(3), 2031–2063. DOI:10.1109/comst.2020.2986024
[15] Kumar, R. S., Raghav, L. P., Raju, D. K., & Singh, A. R. (2021). Intelligent demand side management for opti mal energy scheduling of grid connected microgrids. Applied Energy, 285, 116435. DOI:10.1016/j.apenerg y.2021.116435
[16] Almassalkhi, M., Hiskens, I. A., & Korba, P. (2019). Optimization and control for smart grids: A survey. Ann ual Reviews in Control, 47, 1-17. DOI:10.1016/j.arcontrol.2019.02.002
[17] Xu X，Cao X，Zhao L，et al.2013a.Removal of Cu，Zn，and Cd from aqueous solutions by the dairy ma nure-derived biochar[J].Environmental Science and Pollution Research,20(1):358-368
[18] Wu, K., Li, Q., Chen, Z., Lin, J., Yi, Y., & Chen, M. (2021). Distributed optimization method with weighted gr adients for economic dispatch problem of multi-microgrid systems. Energy, 222, 119898. DOI:10.1016/j.e nergy.2021.119898
[19] Zhu S，Wang S，Yang X，et al.2020.Green sustainable and highly efficient hematite nanoparticles modif ied biochar-clay granular composite for Cr（Ⅵ） removal and related mechanism[J].Journal of Cleaner P roduction,276:123009
[20] Hosseini, S. M., Carli, R., & Dotoli, M. (2020). Robust optimal energy management of a residential microgr id under uncertainties on demand and renewable power generation. IEEE Transactions on Automation Sci ence and Engineering, 18(2), 618–637. DOI:10.1109/tase.2020.2986269
[21] Wan S, Li Y, Cheng S, Zhu S, Di M.2022.Cadmium removal by FeOOH nanoparticles accommodated in bioc har：Effect of the negatively charged functional groups in host[J].Journal of Hazardous Materials,421:126 807
[22] Bonabeau, E. (2002). Agent-based modeling: Methods and techniques for simulating human systems. Pro ceedings of the National Academy of Sciences, 99(suppl_3), 7280–7287. DOI:10.1073/pnas.082080899
[23] Tang X, Shen H, Chen M.2020. Achieving the safe use of Cd- and As-contaminated agricultural land with a n Fe-based biochar: A field study [J]. Science of the Total Environment,706:135898
[24] Zhao, J., Qi, J., Huang, Z., Meliopoulos, A. P. S., Gomez-Exposito, A., Netto, M., Mili, L., Abur, A., Terzija, V., Kamwa, I., Pal, B., & Singh, A. K. (2019). Power System Dynamic State Estimation: Motivations, definition s, methodologies, and future work. IEEE Transactions on Power Systems, 34(4), 3188–3198. DOI:10.1109/ tpwrs.2019.2894769

[25] Zia, M. F., Benbouzid, M., & Elbouchikhi, E. (2018). Microgrid energy management systems: A critical revie w on methods, solutions, and prospects. Applied Energy, 222, 1033-1055. DOI:10.1016/j.apenergy.2018.0 4.103
[26] [J].Chemical Engineering Journal,362:21-29